Article

Cell Reports

Principles of Bacterial Cell-Size Determination Revealed by Cell-Wall Synthesis Perturbations

Graphical Abstract

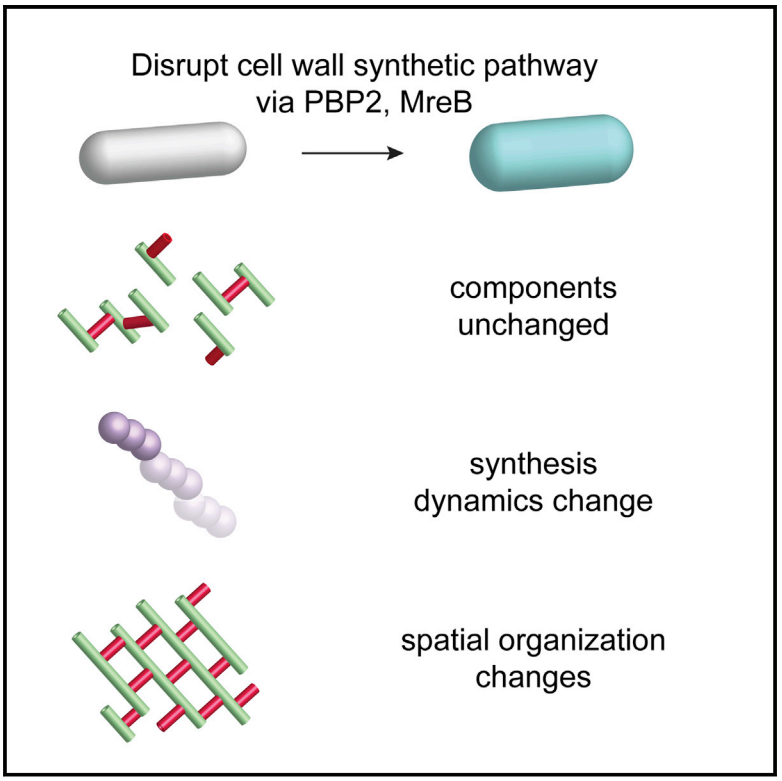

Highlights

Heterologous expression of cell-wall enzymes complements growth and alters cell width

Cell-wall enzyme perturbation does not affect chemical composition of peptidoglycan

Orientation of MreB motion and cell twisting are correlated with cell width

Quantification of growth behaviors reveals different roles for MreB and PBP2

Authors

Carolina Tropini, Timothy K. Lee, ..., Russell D. Monds, Kerwyn Casey Huang

Correspondence

rmonds@syntheticgenomics.com (R.D.M.),
kchuang@stanford.edu (K.C.H.)

In Brief

Tropini et al. demonstrate genetic and chemical means of modulating *E. coli* cell size. They find that wider cells exhibit systematic large-scale changes in cell mechanics consistent with altered chirality and a more isotropic cell wall. Their results highlight the robustness of cell-wall synthesis and physical principles dictating cell-size control.

Tropini et al., 2014, Cell Reports 9, 1520–1527
November 20, 2014 ©2014 The Authors
http://dx.doi.org/10.1016/j.celrep.2014.10.027

OPEN ACCESS
CellPress

Cell Reports
Article

Principles of Bacterial Cell-Size Determination Revealed by Cell-Wall Synthesis Perturbations

Carolina Tropini,[1,2] Timothy K. Lee,[1] Jen Hsin,[1] Samantha M. Desmarais,[1] Tristan Ursell,[1] Russell D. Monds,[1,4,*] and Kerwyn Casey Huang[1,2,3,*]

[1]Department of Bioengineering, Stanford University, Stanford, CA 94305, USA
[2]Biophysics Program, Stanford University, Stanford, CA 94305, USA
[3]Department of Microbiology and Immunology, Stanford University School of Medicine, Stanford, CA 94305, USA
[4]Present address: Synthetic Genomics Inc., 11149 North Torrey Pines Road, La Jolla, CA 92037, USA
*Correspondence: rmonds@syntheticgenomics.com (R.D.M.), kchuang@stanford.edu (K.C.H.)
http://dx.doi.org/10.1016/j.celrep.2014.10.027

SUMMARY

Although bacterial cell morphology is tightly controlled, the principles of size regulation remain elusive. In *Escherichia coli*, perturbation of cell-wall synthesis often results in similar morphologies, making it difficult to deconvolve the complex genotype-phenotype relationships underlying morphogenesis. Here we modulated cell width through heterologous expression of sequences encoding the essential enzyme PBP2 and through sublethal treatments with drugs that inhibit PBP2 and the MreB cytoskeleton. We quantified the biochemical and biophysical properties of the cell wall across a wide range of cell sizes. We find that, although cell-wall chemical composition is unaltered, MreB dynamics, cell twisting, and cellular mechanics exhibit systematic large-scale changes consistent with altered chirality and a more isotropic cell wall. This multiscale analysis enabled identification of distinct roles for MreB and PBP2, despite having similar morphological effects when depleted. Altogether, our results highlight the robustness of cell-wall synthesis and physical principles dictating cell-size control.

INTRODUCTION

The molecular, chemical, and physical mechanisms that control cell shape have been longstanding questions in all kingdoms of life. In bacteria, cell morphology affects many behaviors, such as cell division, motility, nutrient uptake, and biofilm formation (Justice et al., 2008; Young, 2006). Different species adopt a diverse set of morphologies (Young, 2006), although most species can robustly maintain a particular shape. Elucidating the perturbations that adjust morphology and the biophysical mechanisms that transduce these changes to the cellular scale is critically important for our understanding of bacterial physiology.

Bacterial cell shape is conferred by the peptidoglycan (PG) cell wall, a macromolecular polymer network surrounding the cytoplasmic membrane (Schleifer and Kandler, 1972) that is composed of repeating sugar (glycan) subunits crosslinked by short peptides. In Gram-negative bacteria such as *E. coli*, the cell wall is a predominantly single-layered, dynamic meshwork that maintains an approximately constant width as the cell elongates (Scheffers and Pinho, 2005). A major class of proteins involved in the insertion of new PG is the penicillin binding proteins (PBPs), many of whose biochemical activities (transpeptidation, transglycosylation, hydrolysis) have been characterized using liquid chromatography (Banzhaf et al., 2012; Popham and Young, 2003; Vollmer and Bertsche, 2008). Disrupting the function of the PBPs can cause morphologies such as filamentous, coccal, or branched cells (Popham and Young, 2003).

Spatiotemporal coordination of the PBPs has been linked to the cytoskeletal protein MreB, a homolog of eukaryotic actin that polymerizes into filaments that are colocalized with sites of growth (Ursell et al., 2014; White et al., 2010). Depletion of MreB (Carballido-López, 2006; Wachi et al., 1987) or inhibition of MreB polymerization by the small molecule A22 results in progressive cell rounding and eventual lysis (Bean et al., 2009). The recently discovered cell twisting during *E. coli* growth is MreB dependent and is thought to result from chiral ordering of the PG in which the glycan strands have a right-handed orientation bias (Wang et al., 2012). In both *E. coli* and the Gram-positive rod-shaped bacterium *Bacillus subtilis*, MreB moves circumferentially in a directed manner dependent on cell-wall synthesis (Domínguez-Escobar et al., 2011; Garner et al., 2011; van Teeffelen et al., 2011). MreB motion in *E. coli* is reduced by the addition of mecillinam (Lee et al., 2014; van Teeffelen et al., 2011), a beta-lactam antibiotic that specifically inhibits PBP2, an essential transpeptidase encoded by the gene *mrdA* that participates in glycan strand crosslinking. Depletion of wild-type PBP2 causes cell rounding and eventual lysis, similar to MreB depletion (Lee et al., 2014). Given the similar effects of PBP2 and MreB perturbation, these two proteins are often assumed to work in a conserved linear pathway despite the lack of direct evidence (Osborn and Rothfield, 2007).

Even with the identification of many genes and biochemical activities required for cell-wall synthesis, it has been challenging to uncover the principles that unify related mechanisms of cell-shape maintenance and cell-size determination. Since

morphogenesis inherently spans the molecular and cellular scales, a number of factors such as enzyme dynamics and activities, cell-wall chemical composition, spatial organization, and mechanical anisotropy are all potentially important factors. Loss-of-function studies have been invaluable in identifying key necessary activities, but important distinctions between genotype-phenotype relationships are still unresolved. Perturbations that result in graded phenotypic changes to cell width are potentially more useful, as they allow for the discovery of systematic changes in emergent behaviors that suggest a common physical mechanism of cell-width determination.

Here we aim to correlate changes in cell-wall biophysical properties in response to changes in cell geometry that cover a wide, yet physiologically relevant range. We created a library of strains with varied cellular morphologies via heterologous expression of *mrdA* from a range of species. As a complementary means of exploring the morphological phase space, we use sublethal doses of A22 and mecillinam to systematically vary cell size within a single genotype. For these cells, we quantitatively characterize a diverse set of physical and chemical phenotypes, including cell width, elongation rate, response to osmotic shock, and cell-wall composition. Our study demonstrates that heterologous expression and sublethal impairment of cell-wall synthesis can result in subtle modulations in cell width and that these changes are correlated with alterations in peptidoglycan insertion dynamics and cell-wall mechanical properties.

RESULTS

Heterologous Expression of PBP2 in *E. coli* Gives Rise to Distinct Cellular Morphologies

We created an *E. coli* (*Ec*) MG1655 strain deleted for *mrdA* and complemented with *Ec mrdA* expressed from a low-copy plasmid and inducible promoter (Lee et al., 2014) (Table S1). In the absence of inducer, PPB2 levels become limiting after several cell divisions and lysis results (Lee et al., 2014). We then substituted the *Ec mrdA* plasmid with plasmids carrying *mrdA* from a number of species with varying sequence similarity to *Ec* PBP2 (Figure 1A). *mrdA* homologs from *Caulobacter crescentus* (*Cc*) and *Pseudomonas aeruginosa* (*Pa*) (25% and 44% amino acid identity to *Ec* PBP2, respectively) did not complement viability as the sole copy of *mrdA*; depletion of *Ec* PBP2 in cells expressing *Cc* or *Pa mrdA* resulted in cell enlargement and lysis (Figure S1C). However, *mrdA* homologs from *Salmonella typhimurium* (*St*), *Yersinia pseudotuberculosis* (*Yp*), and *Vibrio cholerae* (*Vc*) (96%, 81%, and 56% amino acid identity to *Ec* PBP2, respectively) as the sole source of *mrdA* complemented enough of the *Ec* PBP2 function to support viability (Figures 1B–1D).

Heterologous expression produced a range of cell sizes, with *Vc mrdA* in particular conferring a large increase in cell width and width variability (Figures 1B and 1C); cell length was not substantially affected (Figure 1D). The increased width phenotype of *Vc mrdA* was independent of its expression level (Figure S1D). In a strain with inducible *Ec mrdA* and constitutive *Vc mrdA* (*Ec*/*Vc*), *Ec mrdA* suppressed the effects of *Vc mrdA*, and titrating the expression of *Ec mrdA* yielded graded, stable changes in cell width (Figure 1E). Width also increased when *Ec mrdA* was underexpressed (Figure 1B), similar to previous studies (de Pedro et al., 2001; Popham and Young, 2003). These data suggest that PBP2 interactions with other components of the cell-wall synthesis machinery are sufficiently flexible to tolerate some degree of sequence divergence or fluctuations in expression, although cellular morphology may be altered. In addition, our results suggest that the morphological effects of heterologous expression are enacted through conserved pathways, since expression of *Ec mrdA* suppressed the effects of *Vc mrdA*.

Growth Rate and Cell-Wall Composition Are Maintained as Cell Size Changes

Despite the different cell widths resulting from heterologous *mrdA* expression or altered expression levels of *Ec mrdA*, cells grew at similar rates (Figure S1D). These data indicate that the metabolic functions dictating growth rate were not greatly affected by shape changes resulting from perturbations to PBP2 function.

Given PBP2's essential role in cell-wall synthesis, we sought to determine whether altered PBP2 function affected the chemical composition or degree of crosslinking of the cell wall. We isolated sacculi from each viable heterologous expression strain and cells with low *Ec mrdA* expression and analyzed muropeptide composition using ultra performance liquid chromatography (UPLC; Experimental Procedures) (Lee et al., 2014). Despite the large range of morphological changes (Figure 1), PG composition remained virtually unchanged across all strains and conditions, with no significant differences in either crosslinking or average glycan strand length (Figure 2). These data suggest that the biochemistry of cell-wall synthesis is maintained in addition to cellular growth rate, although cell-wall ultrastructure could vary.

In a previous study, we observed that PG crosslinking was unchanged by treatment with the PBP2 inhibitor mecillinam (Lee et al., 2014). We next investigated whether drug treatments that target the PG synthesis machinery could also result in changes in cell size and serve as a complementary tuning knob to our genetic perturbations. Sublethal concentrations of A22 or mecillinam caused stable changes in average cell width across a population of wild-type *E. coli* MG1655 cells (Figures S1E and S1F). Interestingly, mecillinam-treated cells lost their rod shape at lower widths than A22-treated cells (~1.5 and 2 μm, respectively; Figures S1E and S1F), indicating possible mechanistic differences.

MreB Dynamics Shift Systematically with Increasing Cell Width

To gain insight into how the PG synthesis machinery patterns insertion into the walls of cells with varying widths, we measured the dynamics of MreB clusters by expressing a complementing fusion of *E. coli* MreB to superfolder GFP as the sole copy of MreB at the native chromosomal locus (Figure 3A) (Ursell et al., 2014). We imaged single cells using total internal reflectance fluorescence (TIRF) microscopy and quantified MreB cluster movement based on angle with respect to the longitudinal axis of the cell, speed, and processivity (Figures 3B–3D; Figure S2)

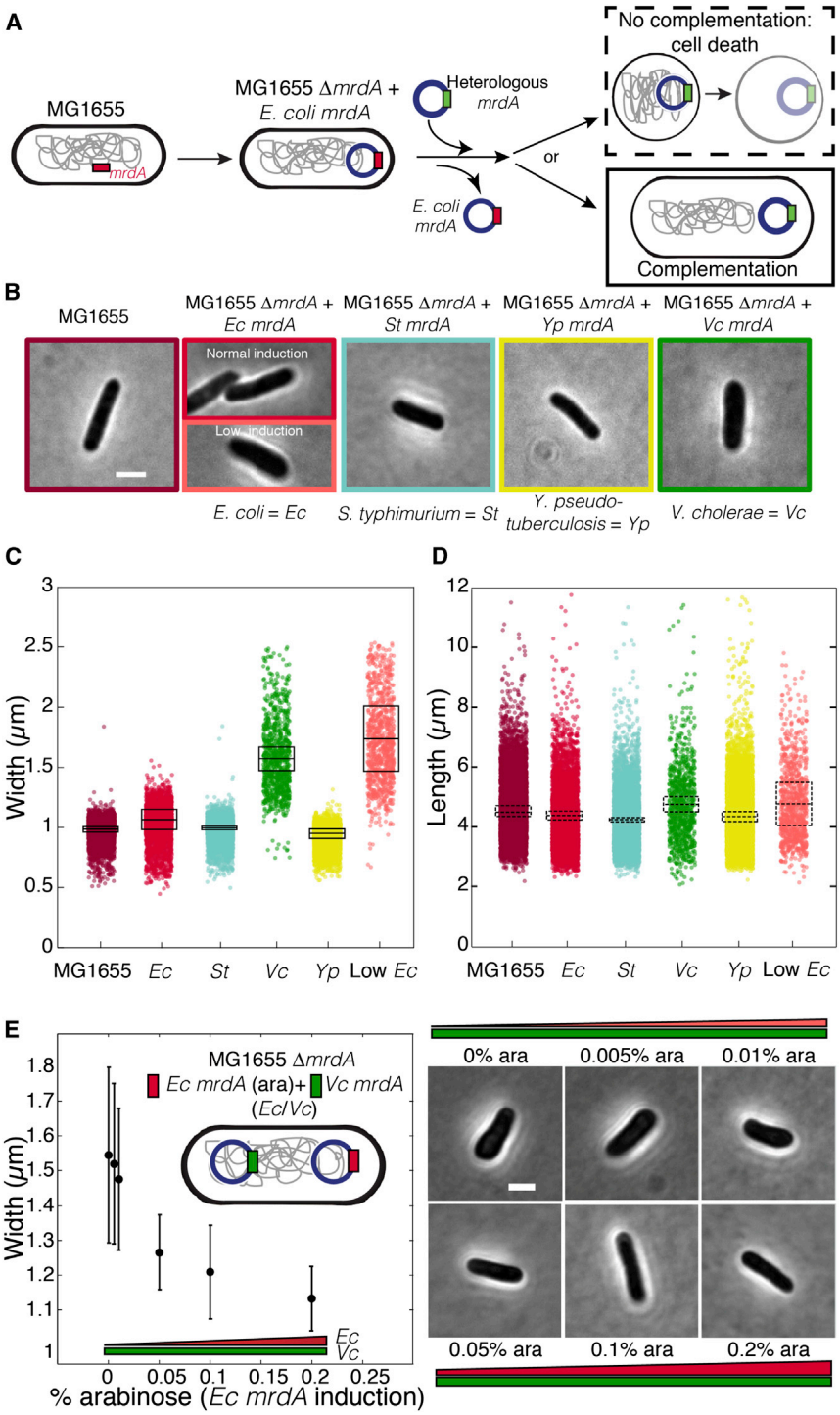

Figure 1. Heterologous Sequences Can Complement the Essential PBP2 Functions in an *E. coli* MG1655 *mrdA* Knockout

(A) Schematic of experimental protocol. Heterologous *mrdA* genes from several species were introduced on an inducible plasmid in an *E. coli* MG1655 *ΔmrdA* strain. Since PBP2 is essential, only heterologous *mrdA* plasmids that successfully complement the native PBP2 function allow proliferation.

(B) Phase-contrast images of complementing heterologous *mrdA* strains (see also Figure S1 for noncomplementing strains).

(C and D) Complementing strains show changes in width (C), but no large differences in length distributions (D). In (C) and (D), boxes define the mean (central bar) and standard deviation (box edges) across three separate experiments. Dots represent single-cell measurements (n = 906–10,902 cells).

(E) *Ec mrdA* suppresses the effect of *Vc mrdA* when the two genes are coexpressed at high levels. Cells expressing *Ec* and *Vc mrdA* controlled by inducible and constitutive promoters, respectively, exhibit a range of stable widths dependent on the level of *Ec* PBP2. Error bars represent standard deviations from the mean.

In (B) and (E), cell width and length closely match the population means. Scale bars, 2 μm.

(Lee et al., 2014). We defined a track as processive if the mean squared deviation fit well to a sum of linear and quadratic terms, as expected in the case of linear, directed motion (Experimental Procedures) (Lee et al., 2014); changing the threshold for goodness of fit did not affect our general conclusions (Figures S2A–S2E). Under sublethal mecillinam treatment, MreB angle was not systematically affected (Figures 3B and S2G). However, in agreement with our previous studies using single MreB^{sw}-PAmCherry molecules (Lee et al., 2014), mecillinam treatment decreased MreB speed (Figures 3C and S2G). A22 treatment does not affect MreB speed (van Teeffelen et al., 2011); however, the angle of MreB motion was correlated with cell width (Figures 3B, 3C, and S2F). Varying the levels of *Ec* PBP2 in *Ec*/*Vc mrdA* cells changed both MreB angle and speed (Figures 3B, 3C, and S2H). For both A22 treatment and induction of *Ec* PBP2 in *Ec*/*Vc mrdA* cells, average MreB angle shifted from >90° to <90° (indicating a change in the average handedness of trajectories), and the spread in the distribution of angles increased (Figures 3B, 3C, and S2F–S2H). Interestingly, in all cases, the fraction of processive MreB decreased with increasing width (Figures 3D and S2F–S2H), indicating that the coordination of PG insertion may be less directed in wider cells; however, it is unknown if diffusive MreB clusters still participate in coordinating PG synthesis. Regardless, the correlations among width, MreB angle, and processive fraction (Figures 3B and 3D) suggest that the spatiotemporal dynamics of cell-wall synthesis shift systematically in wider A22-treated and *Ec*/*Vc mrdA* cells.

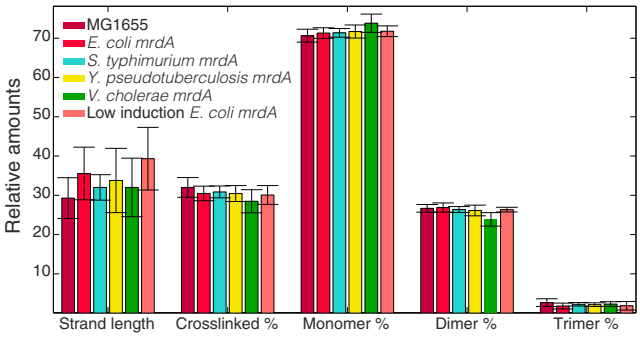

Figure 2. Quantification of PG Content in Heterologous and Underexpressed *E. coli mrdA* Strains

UPLC of PG isolated from cells reveals no significant differences in overall crosslinking levels, average strand length, or relative concentrations of particular chemical species (Experimental Procedures; Table S2). Data are represented as mean ± standard deviation over three separate experiments. The legend color scheme is consistent with that of Figure 1.

TIRF Imaging after Photobleaching Reveals Increased Cell Twisting in Wider Cells

We recently showed that a left-handed pattern of PG insertion (which is guided by MreB) gives rise to a right-handed bias of the glycan strands, which produces the left-handed twisting we observed during the growth of *E. coli* cells (Wang et al., 2012). These twist measurements were obtained by labeling the cell poles with beads and tracking their relative motion as the cell elongates. This method is technically challenging and laborious due to the requirement for bead placement and attachment via optical trapping. We therefore developed a technique (Twist 'n TIRF) to measure growth twist based on bleaching of fluorescent cell-wall label using TIRF microscopy. We previously showed that fluorescent wheat germ agglutinin (flWGA) is a high-affinity, locally stationary cell-surface marker that enables probing of cell-wall growth patterns (Ursell et al., 2014). After uniform flWGA labeling, we used TIRF illumination to selectively photobleach the thin section of the cell wall lying within the TIRF field (extending ~150 nm from the coverslip) (Experimental Procedures; Figure 4A). The cell was then imaged in TIRF as it grew in the absence of label. Twisting of the cell wall during growth results in gradual rotation of the unbleached stain into the field of view, causing an increase in fluorescence. In wild-type cells, we observed progressive fluorescence recovery starting from opposite sides on the two longitudinal halves of the cell, corresponding to left-handed twist (n = 33/33 cells in which twisting was apparent; Figure 4A; Movie S1). We then examined *Vc mrdA* cells using our assay, and surprisingly, we always observed right-handed twist (n = 60/60 twisting cells; Figure 4A; Movie S1).

To relate the cellular fluorescence F to the increase in cell length Δl (Figure 4B), we fit the recovery phase to an experimental growth model function (Experimental Procedures) to extract the rate of fluorescence increase λ (Experimental Procedures; Figure 4B). To predict how fluorescence recovery should be affected by changes in cell width and/or twist angle, we developed a computational model to simulate the spatial dynamics of cell-wall labels due to twisting growth with a fixed angle after photobleaching (Figure 4A; Experimental Procedures). To compare these labeling distributions with our experimental data, we generated simulated fluorescence microscopy images from the 3D positions of wall labels (Experimental Procedures) and then analyzed the simulated images with the same algorithms as our experimental data. We extracted predicted values for λ across a range of widths and twist angles. As expected, simulated cells with higher twist angles had higher values of λ (Figure 4C), since twist dictates the amount of fluorescence entering the field of view as cell length increases. On the basis of our simulated data, we estimated that *Vc mrdA* cells have a higher twist angle (26 ± 4°) than wild-type *E. coli* (13 ± 3°) (Figure 4C), in addition to the previously mentioned reversal in handedness. We also quantified the twist rate in A22- or mecillinam-treated and *Ec/Vc mrdA* cells across a broad range of cell widths (Figures 4D and S3). In A22-treated and *Ec/Vc mrdA* cells, twist angle increased with width in a quantitatively similar manner, suggesting that cell-wall organization is generally altered in these wider cells. Interestingly, mecillinam-treated cells did not show a strong correlation between λ and cell width (Figures 4D and S3B). Consistent with this, mecillinam treatment also affected MreB angle far less than the other treatments. The fact that a variety of perturbations to MreB angle resulted in corresponding changes to twist rate and cell width suggests that MreB angle is mechanistically coupled to these variables.

Given the differential changes in MreB angle and twist rate as cell width increased, we measured the chirality of twist under various conditions (Figure 4E). Consistent with our observed changes in MreB angle (Figure 3B) relative to the circumferential direction (90°), we detected a width-dependent chirality of twist in A22-treated cells and *Ec/Vc mrdA* cells, but not in mecillinam-treated cells (Figure 4E). The fraction of right-handed cells progressively increased as *Ec mrdA* expression was reduced in *Ec/Vc* cells (Figure 4E, left). We also observed a surprising switch from left- to right-handed chirality at ~0.75 μg/mL A22 (Figure 4E, right). In contrast, mecillinam-treated cells showed the same left-handed chirality as wild-type *E. coli* (Figure 4E, middle) across the entire range of accessible widths. These results suggest that changes in MreB angle are strongly coupled with cell wall twisting and chirality, independent of whether the perturbation is to MreB (A22) or PBP2 (*Vc/Ec*). This also illustrates the important point that although perturbing cell-shape pathways may result in similar morphological effects (e.g., cell rounding), the underlying mechanisms are potentially quite different.

Mechanical Response of Wider Cells Suggests Differences in Cell-Wall Organization

Since PG composition remained fixed in our heterologous expression mutants (Figure 2), we hypothesized that changes in cell width might be coupled to alterations in the spatial architecture of the cell wall. We therefore investigated how cellular mechanical properties vary with width by measuring the longitudinal and transverse mechanical strain (fractional stretching) of the cell wall due to turgor pressure. We labeled the cell surface with flWGA (Ursell et al., 2014) and exposed cells to a large (0.5 M) hyperosmotic shock in a microfluidic flow cell (Experimental Procedures; Figure S4). This magnitude of shock caused

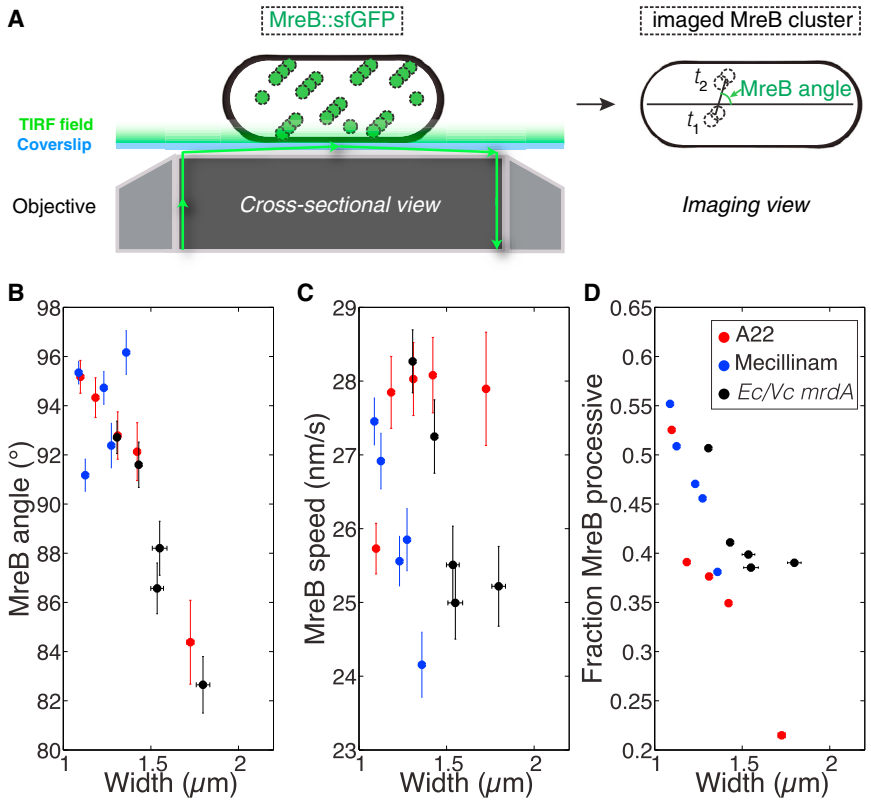

Figure 3. MreB Dynamics Are Affected by Cell Width

(A) Cells with MreB^{sw}-sfGFP as the sole copy of *mreB* were imaged via TIRF microscopy to quantify (B) MreB angle, (C) speed, and (D) fraction of processive MreB molecules (Experimental Procedures). Data in (B)–(D) are mean ± standard error (n = 84–185 cells).

(B) MreB angle is not affected by mecillinam treatment but does exhibit a decrease in average angle and increase in the width of the distribution of angles in both A22-treated and *Ec/Vc* cells.

(C) MreB speed decreases under mecillinam treatment and in *Ec/Vc* cells but is relatively constant under A22 treatment.

(D) In all cases, larger width is coupled to a decreased fraction of processive MreB. See Figure S2 for detailed MreB dynamics.

measureable shrinkage in both length and width (Figure S4A) and resulted in visible plasmolysis (Figure S4B), indicating that the turgor pressure was reduced to zero (Pilizota and Shaevitz, 2012, 2013). Mechanical strain was computed from the fluorescence outline of the cell wall before and after hyperosmotic shock (Figure S4). For wild-type cells, the ratio of circumferential to longitudinal strain was ≈0.5 rather than the value of 2 expected for an isotropic cylindrical shell (Supplemental Information), indicating that more stretching occurs along the longitudinal direction (Figures S4D–S4H). Interestingly, we observed that the ratio increased and approached 1 for wider cells, as would be expected for an isotropic sphere (Supplemental Information and Figure S4C). Taken together, our results suggest that cell widening is coupled to a loss of cell-wall anisotropy.

DISCUSSION

In this study, we systematically varied *E. coli* cell width through heterologous expression of PBP2 sequences and by treating wild-type cells with sublethal levels of drugs that target PBP2 (mecillinam) or MreB (A22). We then examined how biochemical, organizational, and physical attributes of the cell wall scale across a broad range of morphologies and perturbations. This analysis identified general features underlying changes in cell width, such as wider cells exhibiting a more isotropic cell-wall organization and a lower fraction of processive MreB. In addition, we also identified differences in cell-wall chirality that distinguish between MreB and PBP2 perturbation, a key development given that at the morphological level their genotype-phenotype relationships are not resolvable.

The ability to replace an essential enzyme such as PBP2 with homologous proteins implies a remarkable flexibility in the interactions among the components of the cell-wall synthesis machinery. Given that heterologous expression induces changes in morphology (Figure 1), we infer that some aspect of PBP2 functionality must be affected, such as biochemical activity, expression, and/or interactions with other components. How then is growth rate maintained, particularly in strains large increases in cell width? Although it has been assumed that the cell-wall synthesis machinery assembles into a stable complex (Cabeen and Jacobs-Wagner, 2005), we recently demonstrated that PBP2 molecules rapidly diffuse across the cell surface, unlike the directed motion of MreB, indicating that the kinetics of PBP2 activity are not rate limiting for growth (Lee et al., 2014). Thus, growth rate is robust to large changes in both PBP2 abundance and kinetics, consistent with our current observations (Figure S1D).

The dynamic association of PBP2 with MreB-directed glycan insertion (Lee et al., 2014) predicts that muropeptide composition of the cell wall is more robust against perturbations to PBP2 activity. UPLC measurements of cell-wall composition from this study (Figure 2) lend support to this prediction. MreB dynamics in wider cells support the hypothesis that the orientation of newly inserted material is more variable than in wild-type cells, indicating that growth may become less coordinated as width increases (Figure 3B). Furthermore, the increase in diffusive MreB at larger widths (Figure 3D) is consistent with a possible increase in nondirected insertion of peptidoglycan material. Our results also indicate that the effects of PBP2 and MreB inhibition by mecillinam and A22, respectively, lead to larger cells by different mechanisms, despite the similar resulting phenotypes. In the case of A22 treatment, the speed of processive

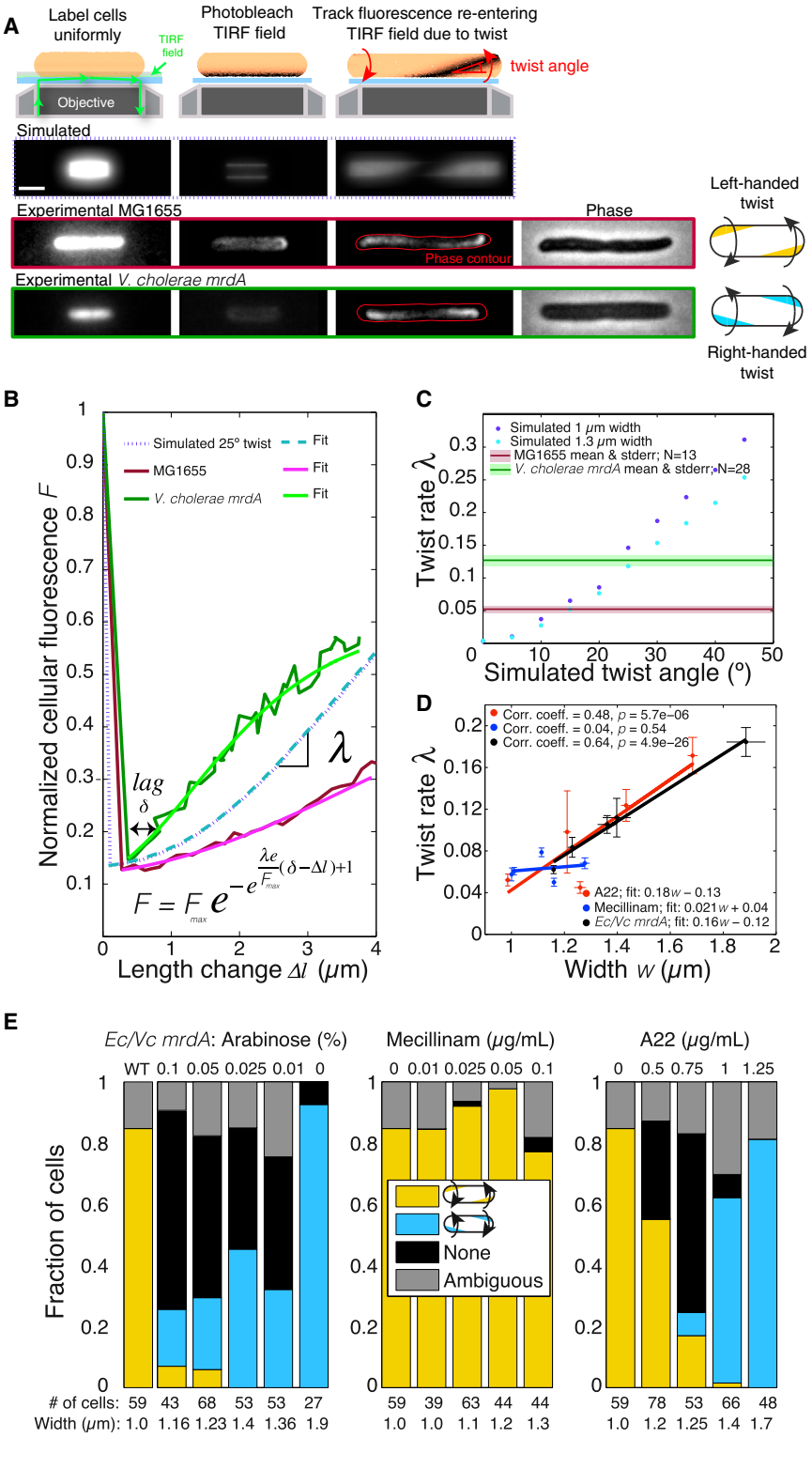

Figure 4. Cell Twisting Properties Change with Cell Width

(A) Cell surfaces were uniformly labeled with fluorescein isothiocyanate–wheat germ agglutinin (fWGA), washed, and imaged in TIRF in the absence of the label and in the presence of cephalexin to prevent cell division (Experimental Procedures). At the beginning of the time-lapse experiment, cells were photobleached. Because of twisting, the unbleached cell wall reentered the TIRF field during elongation; the rate of the fluorescence increase was measured (Movie S1). Scale bar, 2 μm.

(B) Cell outlines were determined from phase-contrast images (A) and used to integrate TIRF fluorescence intensity relative to the prebleached state at each time point. Single-cell fluorescence recovery curves were fitted to a Gompertz equation (Experimental Procedures), where F_{max} is the plateau F level and δ is the lag; the rate of recovery λ was determined for each cell.

(C) Simulated cell twisting and generation of simulated fluorescence images (Experimental Procedures) were used to determine how the cell-twisting angle affects twist rate (λ), which is not very sensitive to width at low twist angles. Experimentally, *Vc mrdA* cells (solid line mean and shaded standard error) had a higher twist angle than wild-type MG1655 cells.

(D) Single-cell twist measurements show a systematic increase in cell twist rate with width (w) in heterologous *Ec/Vc mrdA* and A22-treated cells, but not in mecillinam-treated cells. Data are shown as mean ± standard error in both width and twist rate, with linear fits. Pearson's correlation coefficients are shown.

(E) Twisting chirality changes in heterologous *Ec/Vc mrdA* and A22-treated strains, but not in mecillinam-treated strains, in the manner predicted by the distribution of MreB angles (Figure 3B). Wild-type (WT or 0 μg/ml A22/mecillinam) cells twist with left-handed chirality, while wider *Ec/Vc* or A22-treated cells tend to exhibit right-handed twist. See also Figure S3 and Movie S1 for detailed information.

MreB clusters was not affected, while the orientation of motion and hence presumably PG insertion changed systematically (Figure 3B), leading to opposite twisting chirality at larger widths (Figure 4E); we note that this observation is consistent with our previous finding that cell twisting is abolished at high A22 concentrations, which almost completely depolymerize MreB (Wang et al., 2012). Conversely, mecillinam-treated cells displayed slowed MreB dynamics (Figure 3C) but no change in MreB angle (Figure 3B) or cell-wall twisting chirality (Figure 4E) as width increases. Last, coexpression of heterologous *Vc* PBP2 with varying levels of *Ec mrdA* caused consistent changes to MreB angle (Figure 3B), MreB speed (Figure 3C), and twisting chirality (Figure 4E), indicating that perturbations to PBP2 alone can affect MreB dynamics in multiple ways.

Our TIRF-based assay for measuring twist has higher throughput than our previous optically trapped bead

measurements (Wang et al., 2012), making it feasible to scan collections of mutants. Our measurements of the twist angle for wild-type cells are somewhat higher than our previous bead-based measurements with *E. coli* MC4100 cells at room temperature (~6.5°), which may be due to differences in growth media, temperature, and/or background strain (Wang et al., 2012). Although the physiological function of twisting is currently unknown, we note that it could help to separate daughter cells after cytokinesis or penetrate surfaces. A previous study demonstrated that mixed populations of fluorescent protein-expressing *E. coli* cells separate into sectors as they expand on agar plates, and the sector boundaries exhibit left-handed chirality (Hallatschek et al., 2007). Twisting at the cellular level was hypothesized to be magnified into the handedness of sector boundaries (Hallatschek et al., 2007); our *Vc mrdA* mutant and A22-treated cells could serve as a test of this hypothesized link between cellular handedness and the chirality of colony growth.

Our study also disentangled effects on the chemical construction of the cell wall from downstream effects on cell shape, indicating that changes in PBP2 function perturb cell shape by changing the dynamics of MreB and PG insertion (Figures 4 and S4), rather than PG composition (Figure 2). We cannot exclude the possibility that other enzymes with transpeptidase activity offset any reduction in PBP2 activity in our heterologous PBP2 and mecillinam-treated cells (Popham and Young, 2003); regardless, crosslinking levels were quantitatively maintained even in cells that experienced large changes in morphology (Figure 2; Table S2). Our comparison of the longitudinal and transverse stretching in cells of different sizes suggested that this change might be due to changes in cell-wall molecular organization and anisotropy (Figure S4).

Deconstructing the processes required for establishment of cellular dimensions requires investigations that span many length scales, especially given our results demonstrating that similar morphological phenotypes can belie distinct molecular causation. Future discoveries will rely on the rapid, precise quantification of the physical and dynamic features of morphogenesis, thereby providing a rich, multidimensional phenotype. Ultimately, there are likely several mechanisms to establish a given shape, and the ability to tune cell size through a multitude of chemical and genetic perturbations will be critical for distinguishing between general principles and specific phenomena.

EXPERIMENTAL PROCEDURES

Strains and plasmids used in this study are described in Table S1. For routine culturing, cells were grown in lysogeny broth consisting of tryptone (1% w/v), yeast extract (0.5% w/v), and NaCl (0.5% w/v) and supplemented with the appropriate inducer and antibiotic.

For fluorescence imaging, cells were grown in EZ-RDM+0.2% glucose. Strains were grown at 37°C unless stated otherwise. Custom MATLAB (MathWorks) image-processing code was used to segment cells and to identify cell outlines from phase-contrast microscopy images (Ursell et al., 2014).

Ultra performance liquid chromatography of peptidoglycan composition was performed as previously described (Brown et al., 2012; Desmarais et al., 2014).

Descriptions of other Experimental Procedures can be found in the Supplemental Information.

SUPPLEMENTAL INFORMATION

Supplemental Information includes four figures, two tables, and one movie and can be found with this article online at http://dx.doi.org/10.1016/j.celrep.2014.10.027.

AUTHOR CONTRIBUTIONS

C.T., T.K.L., J.H., S.M.D., R.D.M., and K.C.H. designed the experiments. C.T. and T.K.L. executed the experiments. C.T., T.K.L., J.H., S.M.D., and T.U. performed the analyses. All authors contributed to writing the paper.

ACKNOWLEDGMENTS

The authors thank Daniel Fisher, Julie Theriot, Steve Quake, members of the K.C.H. lab, Ned Wingreen, and Joshua Shaevitz for helpful discussions. We also thank Mats Hidestrand, Krystal St. Julien, and Danielle Swem for help with strain construction and the Dueber lab for providing plasmid backbones. This work was supported by a Stanford Interdisciplinary Graduate Fellowship and a Stanford Graduate Fellowship (to C.T.), a Siebel Scholars Graduate Fellowship (to T.K.L.), support from an NIH Biotechnology Training Grant (to T.K.L.), a Bio-X Senior Postdoctoral Fellowship (to R.D.M.), NIH Ruth L. Kirschstein National Research Service Award 1F32GM100677-01A1 (to J.H.), a Stanford School of Medicine Dean's Postdoctoral Fellowship (to J.H.), and NIH Director's New Innovator Award DP2OD006466 (to K.C.H.).

Received: May 12, 2014
Revised: August 21, 2014
Accepted: October 13, 2014
Published: November 6, 2014

REFERENCES

Banzhaf, M., van den Berg van Saparoea, B., Terrak, M., Fraipont, C., Egan, A., Philippe, J., Zapun, A., Breukink, E., Nguyen-Distèche, M., den Blaauwen, T., and Vollmer, W. (2012). Cooperativity of peptidoglycan synthases active in bacterial cell elongation. Mol. Microbiol. *85*, 179–194.

Bean, G.J., Flickinger, S.T., Westler, W.M., McCully, M.E., Sept, D., Weibel, D.B., and Amann, K.J. (2009). A22 disrupts the bacterial actin cytoskeleton by directly binding and inducing a low-affinity state in MreB. Biochemistry *48*, 4852–4857.

Brown, P.J.B.P., de Pedro, M.A.M., Kysela, D.T.D., Van der Henst, C., Kim, J., De Bolle, X., Fuqua, C., and Brun, Y.V.Y. (2012). Polar growth in the Alphaproteobacterial order Rhizobiales. Proc. Natl. Acad. Sci. USA *109*, 1697–1701.

Cabeen, M.T., and Jacobs-Wagner, C. (2005). Bacterial cell shape. Nat. Rev. Microbiol. *3*, 601–610.

Carballido-López, R. (2006). The bacterial actin-like cytoskeleton. Microbiol. Mol. Biol. Rev. *70*, 888–909.

de Pedro, M.A.M., Donachie, W.D.W., Höltje, J.V.J., and Schwarz, H. (2001). Constitutive septal murein synthesis in *Escherichia coli* with impaired activity of the morphogenetic proteins RodA and penicillin-binding protein 2. J. Bacteriol. *183*, 4115–4126.

Desmarais, S.M., Cava, F., de Pedro, M.A., and Huang, K.C. (2014). Isolation and preparation of bacterial cell walls for compositional analysis by ultra performance liquid chromatography. J. Vis. Exp. *15*, e51183.

Domínguez-Escobar, J., Chastanet, A., Crevenna, A.H., Fromion, V., Wedlich-Söldner, R., and Carballido-López, R. (2011). Processive movement of MreB-associated cell wall biosynthetic complexes in bacteria. Science *333*, 225–228.

Garner, E.C., Bernard, R., Wang, W., Zhuang, X., Rudner, D.Z., and Mitchison, T. (2011). Coupled, circumferential motions of the cell wall synthesis machinery and MreB filaments in *B. subtilis*. Science *333*, 222–225.

Hallatschek, O., Hersen, P., Ramanathan, S., and Nelson, D.R.D. (2007). Genetic drift at expanding frontiers promotes gene segregation. Proc. Natl. Acad. Sci. USA *104*, 19926–19930.

Justice, S.S.S., Hunstad, D.A.D., Cegelski, L., and Hultgren, S.J.S. (2008). Morphological plasticity as a bacterial survival strategy. Nat. Rev. Microbiol. *6*, 162–168.

Lee, T.K., Tropini, C., Hsin, J., Desmarais, S.M., Ursell, T.S., Gong, E., Gitai, Z., Monds, R.D., and Huang, K.C. (2014). A dynamically assembled cell wall synthesis machinery buffers cell growth. Proc. Natl. Acad. Sci. USA *111*, 4554–4559.

Osborn, M.J.M., and Rothfield, L. (2007). Cell shape determination in *Escherichia coli*. Curr. Opin. Microbiol. *10*, 606–610.

Pilizota, T., and Shaevitz, J.W. (2012). Fast, multiphase volume adaptation to hyperosmotic shock by *Escherichia coli*. PLoS ONE *7*, e35205.

Pilizota, T., and Shaevitz, J.W. (2013). Plasmolysis and cell shape depend on solute outer-membrane permeability during hyperosmotic shock in *E. coli*. Biophys. J. *104*, 2733–2742.

Popham, D.L., and Young, K.D. (2003). Role of penicillin-binding proteins in bacterial cell morphogenesis. Curr. Opin. Microbiol. *6*, 594–599.

Scheffers, D.-J., and Pinho, M.G. (2005). Bacterial cell wall synthesis: new insights from localization studies. Microbiol. Mol. Biol. Rev. *69*, 585–607.

Schleifer, K.H., and Kandler, O. (1972). Peptidoglycan types of bacterial cell walls and their taxonomic implications. Bacteriol. Rev. *36*, 407–477.

Ursell, T.S., Nguyen, J., Monds, R.D., Colavin, A., Billings, G., Ouzounov, N., Gitai, Z., Shaevitz, J.W., and Huang, K.C. (2014). Rod-like bacterial shape is maintained by feedback between cell curvature and cytoskeletal localization. Proc. Natl. Acad. Sci. USA *111*, E1025–E1034.

van Teeffelen, S., Wang, S., Furchtgott, L., Huang, K.C., Wingreen, N.S., Shaevitz, J.W., and Gitai, Z. (2011). The bacterial actin MreB rotates, and rotation depends on cell-wall assembly. Proc. Natl. Acad. Sci. USA *108*, 15822–15827.

Vollmer, W., and Bertsche, U. (2008). Murein (peptidoglycan) structure, architecture and biosynthesis in *Escherichia coli*. Biochim. Biophys. Acta *1778*, 1714–1734.

Wachi, M., Doi, M., Tamaki, S., Park, W., Nakajima-Iijima, S., and Matsuhashi, M. (1987). Mutant isolation and molecular cloning of mre genes, which determine cell shape, sensitivity to mecillinam, and amount of penicillin-binding proteins in *Escherichia coli*. J. Bacteriol. *169*, 4935–4940.

Wang, S., Furchtgott, L., Huang, K.C., and Shaevitz, J.W. (2012). Helical insertion of peptidoglycan produces chiral ordering of the bacterial cell wall. Proc. Natl. Acad. Sci. USA *109*, E595–E604.

White, C.L., Kitich, A., and Gober, J.W. (2010). Positioning cell wall synthetic complexes by the bacterial morphogenetic proteins MreB and MreD. Mol. Microbiol. *76*, 616–633.

Young, K.D. (2006). The selective value of bacterial shape. Microbiol. Mol. Biol. Rev. *70*, 660–703.